Chemical Engineering Journal 444 (2022) 136421

Contents lists available at ScienceDirect

Chemical Engineering Journal

journal homepage: www.elsevier.com/locate/cej

Polyrotaxane based leakage-proof and injectable phase change materials with high melting enthalpy and adjustable transition temperature

Guang-Zhong Yin [a,b], Alba Marta López [a], Xiao-Mei Yang [a], Xiang Ao [a], Jose Hobson [a], De-Yi Wang [a,b,*]

[a] IMDEA Materials Institute, C/Eric Kandel, 2, 28906, Getafe, Madrid, Spain
[b] Universidad Francisco de Vitoria, Ctra. Pozuelo-Majadahonda Km 1, 800, 28223, Pozuelo de Alarcón, Madrid, Spain

ARTICLE INFO

Keywords:
Phase change materials
Thermal management
Injectable
Green pathway

ABSTRACT

In this work, a series of advanced phase change materials (PCMs) were fabricated by using polyrotaxane (PLR) as supports for encapsulating poly (ethylene glycol) (PEG). Phase-change enthalpy is mainly regulated by the PEG contents, whereas phase change temperature is controlled by PEG molecular weight. All PCMs have good form stabilities due to the good compatibility between PLR and PEG, and supporting ability of PLR. Given that the PLR support itself has phase-transition properties, the resulting composites have high phase change enthalpies (116.1–162.2 J g^{-1}) and very high enthalpy efficiency (>100%). It is a green and efficient preparation method because the whole preparation process did not involve organic solvents, and the material was prepared at room temperature. In addition, the obtained PCMs can be easily extruded and re-molded, which provides technical premise and convenience for the large-scale applications. As a typical application example, the PCMs showed its significant advantages in simulated solid-state disk model temperature regulation, which fully demonstrates the practical and superior application value of the PCMs in the field of thermal management for electronic devices.

1. Introduction

To improve the efficiency of electronical devices thermal management, phase change materials (PCMs) attract lots of attention due to their high thermal energy storage capacity, adjustable working temperature range, and long-term stability.[1–3] However, the common issues of organic PCMs are their poor flexibility, and leakage during phase-change process. [4–6] To solve these problems, some porous support materials have usually been incorporated with organic PCM working substance to improve their form stability and realize solid–solid phase change. Generally, the traditional form stable PCMs use aerogel [2], microcapsules[7] and some other polymers (with high melting point [8] but no phase change effect when reaching the PCM substance melting temperature) to support the structure of the PCMs. [9] In order to prevent the leakage of PCMs, these composites often use materials without phase change ability as support materials. Therefore, while obtaining form stability, the PCMs also lose energy storage capacity. There are two reasons for the losing of thermal storage capacity: (1) the energy storage capacity of the composite is reduced by the support material without phase change ability; (2) the PCM is bound by the support material in a narrow space, and some of the chain segments cannot crystallize and melt normally and efficiently, which further reduces the energy storage capacity of the PCMs. Therefore, the enthalpy efficiency of conventional PCM is usually lower than 100%. We think that the support materials with typical phase transition behavior and suitable phase transition temperature should be selected as one of the effective ways to solve the problem of enthalpy capacity losing.

In addition, the PCMs prepared by traditional methods also have some typical deficiencies. For example, PCMs prepared by microcapsule method usually have relatively low dimension and is necessary to be further encapsulated for practical application. Furhermore, the enthalpy of phase transition may decrease greatly [10]. Convertional polymer based PCM also faces common challenges, such as low encapsulation efficiency, low enthalpy and consuming of organic solvents. [11] Most of the conventional methods are difficult to achieve convenient and repeatable processing. Especially, the 3D porous materials loaded PCM is usually difficult to achieve flexibility and re-molding. [12–14] These shortcomings limit their wide application, because the realization of

* Corresponding author at: IMDEA Materials Institute, C/Eric Kandel, 2, 28906, Getafe, Madrid, Spain.
E-mail address: deyi.wang@imdea.org (D.-Y. Wang).

https://doi.org/10.1016/j.cej.2022.136421
Received 20 October 2021; Received in revised form 22 March 2022; Accepted 12 April 2022
Available online 20 April 2022

repeated processing or plastic processing of PCM can facilitate the mass-production for the wide application.

The PCMs thermal regulation market on the mobile phone, computer and other mobile terminals is in full bloom under 5G era. The application of renewable materials is currently considered as a necessity for sustainable develoment. [15,16] Therefore, developing ecofriendly energy management materials is vital for sustainable research.[17].

Polyethylene glycol (PEG)-based PCMs are widely used as PCM work sbstance in the fields of solar energy harvesting and waste heat recovery. [18] The supporter materials with typical phase transition behavior in the shape-stabilized PCMs have been reported. For example, polymeric solid–solid PCMs were used as the supports of shape-stabilized PCMs in some literatures: Novel form stable phase change materials based on the composites of polyethylene glycol/polymeric solid–solid phase change material.[19] Form-stable phase change materials with high phase change enthalpy from the composite of paraffin and cross-linking phase change structure. [20] Binary shape-stabilized phase change materials based on poly(ethylene glycol)/polyurethane composite with dual-phase transition.[21] Polyrotaxane (PLR) has good processability and high shape stability. [22] Integrating the typical disadvantages of traditional PCM and the requirements of PCM advanced processing and green manufacturing, in this work, we will choose the highly flexible PLR as the support materials, because the molecular chain of PLR is almost the same as PEG, and PLR itself is also a PCM with excellent performance, especially the form stability. We believe that it will be an ideal support material for PEG based PCMs. So as to ensure that the final PCMs have the following advantages: (1) good durability, high enthalpy efficiency after melting and cooling process, (2) indicating excellent leakage proof performance, and (3) green and convenient processability and reprocess ability, which provides practical basis for the wide application of the corresponding PCMs.

2. Results and discussion

2.1. Preparation, form stability and mechanical performance of PCM

Fig. 1a shows the two-step process of the PCMs preparation. The synthesis of PLR as the step 1 is reported in previous work. [22] The experimental section is provided in the Supplementary data. The structure of PLR can be confirmed by ^{1}H nuclear magnetic resonance, Fourier transform infrared spectroscopy and solubility (Figure S1-S3). For the step 2, the PEG solution (including PEG 1k, PEG 1.5k or PEG 6k) was directly mixed and stirred with the newly prepared PLR solution. The specific component contents are shown in Table S1. The selected proportions of PLR/PEG6k PCM are 30 wt%, 60 wt%, 90 wt%, 120 wt%, 150 wt%, 200 wt%, 250 wt%, 300 wt% and 350 wt%, in order to regulate the phase change enthalpy. The obtained sample sheets with different thickness can be realized by hot press. Fig. 1b shows the XRD curve of sample PPEG6-150. The XRD curves of other samples are all provide in Figure S4–S5 . As it can be seen, PEG shows two peaks at 19.2° and 23.3°, which are attributed to crystal planes (1 2 0) and concerted (1 1 2)/(0 3 2) planes, respectively. [23] In addition, the characteristic peaks at 2θ = 5.37°, 7.44°, 10.84°, and 12.10° were observed (Fig. 1b). The values are almost the same as those reported in a past report: 5.30° (0 0 1), 7.41° (1 0 0), 10.9° (0 0 2), and 12.8° (1 1 0) obtained from the dried PLR crystal consisting of α-Cyclodextrin (α-CD) and PEO, [24] which is termed as α-CD crystal unit (in this work) as shown in Fig. 1a (see the blue rectangle shape). These α-CD crystal units may well

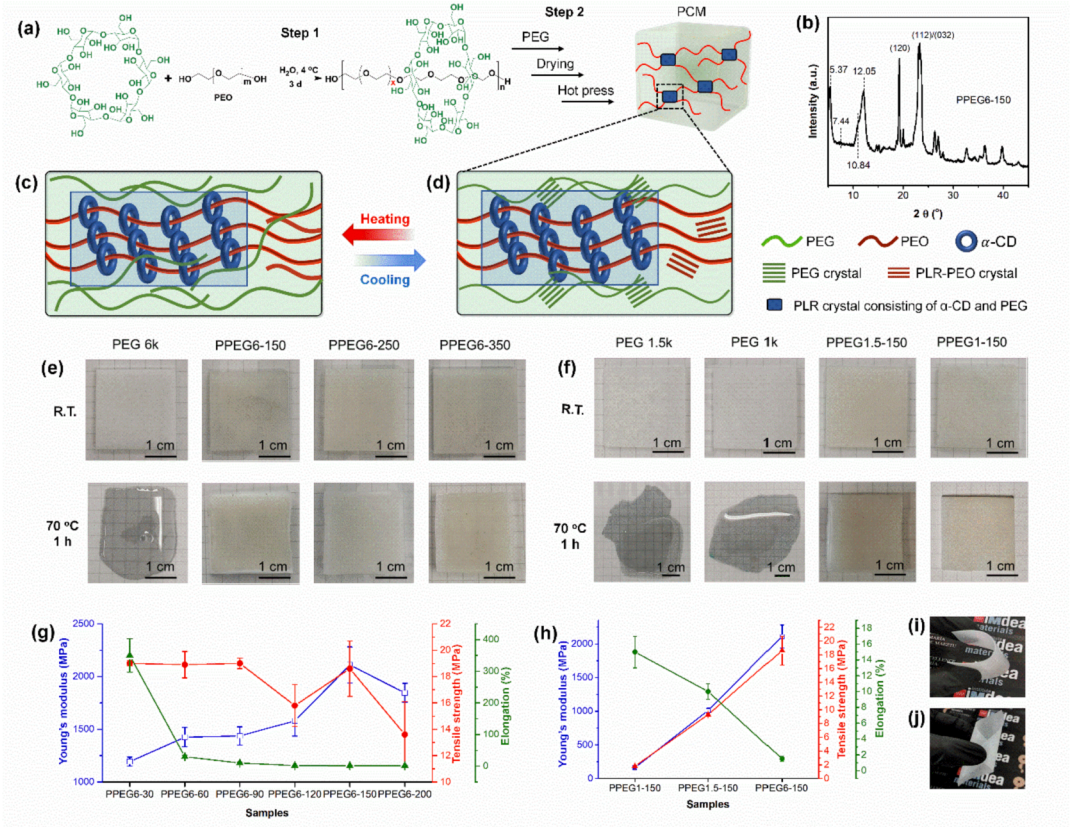

Fig. 1. (a) PCM preparation routes: step 1, synthesis of PLR and step 2, encapsulation of PEG, (b) XRD curve of typical sample PPEG6-150, (c) diagram of melting state of the PCM, (d) diagram of crystallization state of the material at room temperature, (e) schematic diagram of form stability test for representative samples: PEG6k, PPEG6-150, PPEG6-250 and PPEG6-350, (f) form stability test of the samples: PEG 1 k, PEG 1.5 k, PPEG1-150 and PPEG1.5–150, (g) mechanical properties of sample PPEG6-30, PPEG6-60, PPEG6-90, PPEG6-120, PPEG6-150 and PPEG6-200, (h) mechanical properties of sample PPEG1-150, PPEG1.5–150 and PPEG6-150, and flexible schematic diagram of PPEG1-150 sheet (thickness ~ 0.5 mm) with (i) folded shape and (j) curled shape.

maintain in a certain temperature range, so as to act as a physical cross-linking point. The microstructure is further shown in Fig. 1c and Fig. 1d. During the phase transformation, the free segments of PEO or PEG melt and crystallize, and the shape stability of PCM is guaranteed by the α-CD crystal units or entanglement of PEO molecular chains. The photos of pure PEG and PLR/PEG using hot plate treatment at different temperature are shown in Fig. 1e-f. PEG fully melted at 70 °C in 1 h, but all the PLR/PEG PCMs showed no significant appearance changes. There is no leakage and shape change during the heating, which indicates that the PLR/PEG PCMs have good form stability. (Figure S6).

It was found that the PPEG0.6–150, PPEG0.6–40 and PPEG0.4–150 showed significant leakage, as shown in Figure S7. Since PEG 1k and PEG 1.5k have no leakage at 70 °C for a long time (Fig. 1f), we can assign that increasing the molecular weight is conducive to avoid PEG substance leakage. Therefore, it is suggested that the molecular weight of PEG should be higher than that of PEG 1k (Mn = 1304 g mol^{-1}, PDI = 1.04) in current material system.

We have carried out tensile mechanical tests on the series of PPEG6k samples. The key parameters are all presented in Fig. 1g and Fig. 1h. Detailed mechanical data are listed in Table S2. Concretely, as shown in Fig. 1g, with the increase of PEG 6k content, Young's modulus increased, while tensile strength and elongation% decreased. We choose 150% as the load ratio for analyzing the influence of molecular weight on mechanical performance. As shown in Fig. 1h, the molecular weight of PEG increased, Young's modulus and tensile strength were significantly increased, and elongation at break decreased. The changes of these mechanical properties are affected by the aggregation morphology of PCM such as molecular weight and molecular crystallization.

Furthermore, we cut the sample to 50 mm × 40 mm × 0.5 mm, and the flexibility was tested simply by bending with two fingers. As shown in Fig. 1g, the elongation decreases with the increase of PEG6k (from 30 wt% to 350 wt%). When the content of PEG is higher than 300 wt%, the material can hardly be bent (but the material still has good leakage resistance and mechanical support, see Section 2.5 and the related sample PPEG6-350). Sample PPEG1-150 and PPEG1.5–150 are endowed with ultra-high flexibility due to their low T_m (see Fig. 1i, 1j and Figure S8). The bending images of other samples are shown in Figure S9.

2.2. Phase change process of the PCM

We observed the crystal morphology of typical samples by polarized optical microscopy. Fig. 2a-c correspond to the spherulite morphologies of PPEG6-150, PPEG1.5–150 and PPEG1-150, respectively. A typical spherocrystal pattern was observed for all the three selected samples. The particle size distribution for sample PPEG6-150 is shown in Fig. 2a inset, with an average particle size of ~ 220 μm and unimodal

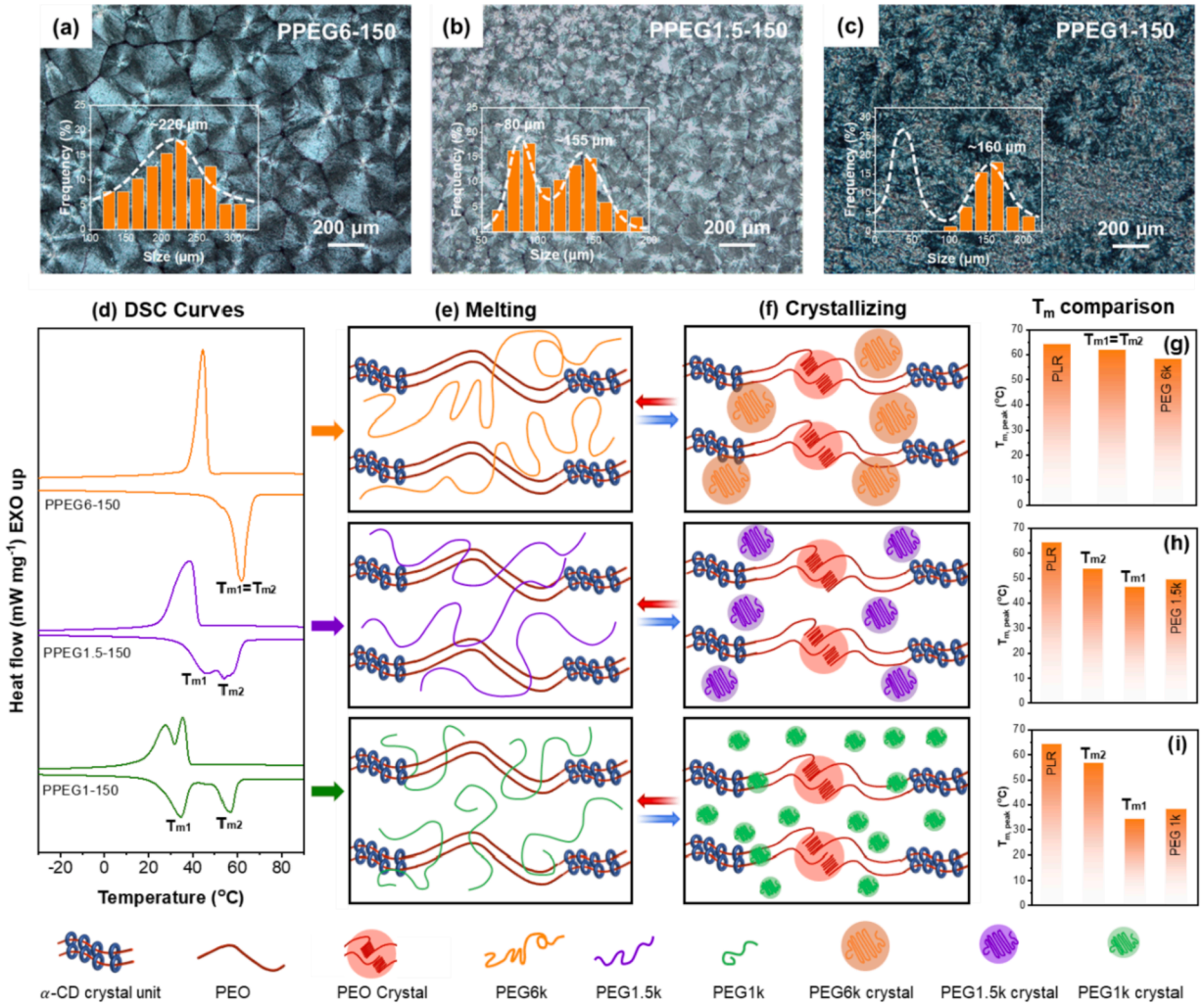

Fig. 2. POM image, crystal size and distribution of (a) PPEG6-150, (b) PPEG1.5–150, (c) PPEG1-150, (d) DSC curves of sample PPEG6-150, PPEG1.5–150 and PPEG1-150, (e) melting status of PPEG6-150 (top), PPEG1.5–150 and PPEG1-150 (bottom), (f) Crystal status of PPEG6-150 (top), PPEG1.5–150 and PPEG1-150 (bottom), (g) melting temperature ($T_{m,peak}$) of sample PLR, PEG 6 k, and PPEG6-150, (h) melting temperature of samples PLR, PPEG1.5–150 (two peaks) and PEG 1.5 k, and (i) melting temperature of samples PLR (T_m = 64.40 °C [20]), PPEG1-150 (two peaks) and PEG 1 k.

distribution. A spherocrystal pattern similar to that for PPEG6-150 was also observed for sample PPEG1.5–150 (Fig. 2b), however, the spherocrystal size were much smaller than those of the PPEG6-150. In addition, the spherulite size shows a relatively continuous bimodal distribution (peak 1 at 155 μm and peak 2 at 80 μm). No homogeneous spherocrystal patterns were observed for sample PPEG1-150. In Fig. 2c, large spherulites (~160 μm) and very small spherulites coexist. Due to the limitation of software and image definition, the particle size distribution in small size range cannot be given reasonably (Fig. 2c inset). The Gibbs-Thomson equation [25] predicts that the melting point depression melting temperature (T_m) for a crystal of size d_c [m] is given by the following equation:

$$T_m = T_m^0 - \frac{2\sigma T_m^0}{d_c \rho_c \Delta H^0} \quad (1)$$

where, σ [J m^{-2}] is the surface energy of the interface, T_m^0 is the equilibrium melting temperature, T_m [^{o}C] is the melting point of crystals of size d, ΔH^0 [J g^{-1}] is the bulk enthalpy of fusion, and ρ_c [kg m^{-3}] is the density of the solid. According to equation (1), the smaller crystal size has lower melting point. Therefore, the size and distribution of the grains in Fig. 2a-c directly determine the DSC scanning curve of the samples (Fig. 2d). In sample PPEG6-150, PEG 6k and PLR can form spherulites with relative uniform size, and thus show a significant single peak distribution (in both crystallization and melting process). The other two samples show bimodal melting behaviors. This is mainly due to the significant crystal size and distribution differences. DSC data of other samples are shown in Figure S10-S21. The crystallinity data are listed in Table S3. It can be found that the crystallinity of the samples generally remains at a high level of > 75%, which is also the practical premise to ensure that high enthalpy of PCM.

Based on the above experimental results, we can interpret the phase transition process of this series of phase change materials in detail. When the temperature is below the melting temperature of α-CD crystal units, the α-CD crystal unit will maintain. According to the previous reports, the melting point of α-CD crystal unit is 98.32°C. [22] Therefore, the shape of the material can be well maintained at 70 °C (the form stability test temperature) in this study. In other words, the α-CD crystal unit will be stable at the melting temperature of PEG or PEO. During the heating process, PEG molecules form random molecular chains, and PEG does not leak due to the restriction of PLR frameworks (Fig. 1e and 1f) during the heating process. Concretely, as shown in Fig. 2e, 2f (in sample PPEG6-150), the crystallization of PEG and PLR was almost synchronous to form relatively large and uniform spherulites. For the PPEG1-150 and PPEG1.5–150, because of its low crystallization temperature, it is necessary to start crystallization when the PLR crystallization reaches a certain degree. The delayed crystallization of PEG will complete crystallization in the confined space. PLR was also affected by the impurities of low molecular PEG in the crystallization process, and when PEG began to crystallize, there was a competitive relationship between PLR and PEG crystallization. As a result, the melting points of both PLR and PEG in PLR were significantly lower than those of pristine PLR and pure PEG, respectively, as shown in Fig. 2g-i and the following formulas, $T_{m,PEG6k} < T_{m1} = T_{m2} < T_{m,PLR}$ (for sample PPEG6-150), and $T_{m1} < T_{m,PLR}$, and $T_{m2} < T_{m,PEG}$ (for both sample PPEG1.5–150 and PPEG1-150), where T_{m1}, T_{m2} are the melting temperature of PLR and PEG in PCMs (as shown in Fig. 2d), respectively, and $T_{m,PLR}$, $T_{m,PEG}$ are the peak melting temperature of pristine PLR (64.40 °C) and pure PEG (PEG 6k, PEG 1.5k and PEG 1k), respectively.

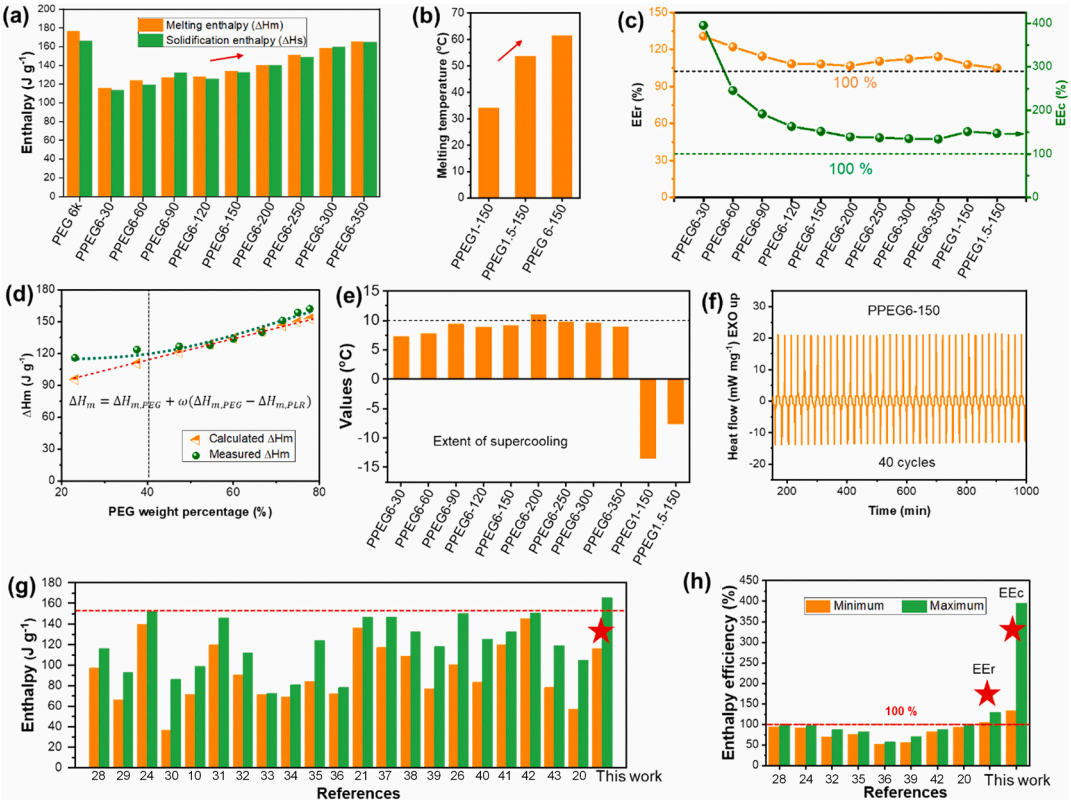

Fig. 3. (a) Enthalpy results of all PEG 6 k related samples, (b) melting temperature (T_{m1} that is obtained from DSC curve) of samples PPEG1-150, PPEG1.5–150 and PPEG6-150, (c) enthalpy efficiency (both EEr and EEc), (d) the measured and calculated values of enthalpy, (e) extent of supercooling of all the PCM samples, (f) the cycle performance of PPEG6-150 as a typical example. The cycle performance of some other samples (PPEG6-90 and PPEG6-350) is shown in Figure S22. Comparation for (g) latent heat and (h) enthalpy efficiency to the reports elsewhere.

2.3. PCM performance

2.3.1. Thermal storage and cycling performance

We can control the latent heat of phase transition by adding different amounts of PEG. As shown in Fig. 3a, the enthalpy increases with the increase of PEG 6k contents. The phase transition enthalpy of sample PPEG6-350 can be as high as 162.2 J g^{-1} when the addition amount reaches 350% (w_{PEG} = 77.8 wt%). We can also adjust the phase transition temperature of PCM by changing the molecular weight of PEG. As shown in Fig. 3b, by adding PEG 1k, PEG 1.5k or PEG 6k, the peak temperature of phase transition can be regulated from ~ 30 °C to ~ 60 °C. Furthermore, the conventional enthalpy efficiency (EEc) of PCMs can be determined by equation (2), [26,27].

$$EEc\% = \frac{\Delta H_m}{\omega \Delta H_{m,\ PCM}} \times 100\% \quad (2)$$

where, ΔH_m [J g^{-1}] is the enthalpy value of the target PCMs. $\Delta H_{m,\ PCM}$ [J g^{-1}] represents the enthalpy of PCM substance, namely, PEG, and ω [%] is the mass ratio of PEG in the PCMs. While the real enthalpy efficiency (EEr) of the PCM can be determined by equation (3),

$$EEr\% = \frac{\Delta H_m}{\omega \Delta H_{m,PCM} + (1-\omega)\Delta H_{m,Support}} \times 100\% \quad (3)$$

where, ω [%] is the weight content of PEG, $\Delta H_{m,\ PCM}$ [J g^{-1}] is the enthalpy of PEG, and $\Delta H_{m,\ Support}$ [J g^{-1}] is the melting enthalpy of PLR. In the conventional case, the supporter does not contribute to the enthalpy, that is to say $\Delta H_{m,\ Support} = 0$. Therefore, $EEc\% = EEr\%$. However, PLR plays a dual role in this research, namely, both supporter and PCM substance, thus, $EEc\% > EEr\%$ (Fig. 3c).

The heat loses and ΔH_s were calculated and listed in Table S3. The PCMs exhibited a high enthalpies (116.1 ~ 162.2 J g^{-1}, Fig. 3a) and high enthalpy efficiency. In addition, the specific calculation formula for calculated enthalpy ($\Delta H_{m,\ Cacld.}$) is as follows,

$$\Delta H_{m,Cacld.} = \Delta H_{m,PLR} + \omega(\Delta H_{m,PEG} - \Delta H_{m,PLR}) \quad (4)$$

where, $\Delta H_{m,PEG}$ [J g^{-1}] and $\Delta H_{m,PLR}$ [J g^{-1}] are the enthalpy of PEG and PLR, respectively, and ω [%] is the weight percentage of PEG in the target PCMs. It is found that the calculated value of phase transition enthalpy is in good agreement with the measured value when PEG is with certain region (from ~ 40 wt% to ~ 80 wt%) (Fig. 3d), which indicates the solidification of PLR and PEG is relative independent within these compositions. The corresponding data are listed in Table 1 and shown in Fig. 3d. The extent of supercooling (ΔT, °C) was calculated by equation (5):

$$\Delta T = T_{m,onset} - T_{s,onset} \quad (5)$$

where, $T_{m,onset}$ [°C] is onset temperature of melting and $T_{s,onset}$ [°C] is onset temperature of solidification. Based on equation (5), ΔT of the PCMs encapsulating PEG 6 k are all calculated to be ~ 10 °C (Table 1). As shown in Fig. 3e, negative supercooling occurs for both sample PPEG1-150 and PPEG1.5–150. The negative value is calculated according to the definition formula (5). Because the macro spherulite component of the material melts later and crystallizes first. In this way, there is a significant overlap temperature zone between the crystallization process and the melting range, so the negative index can be obtained based on equation (5). This shows that the supercooling can be eliminated by blending PEG with different molecular weight on the basis of the definition formula (5).

Fig. 3f shows the cycle curves of the typical sample PPEG6-150. After 40 cycles, the material still shows a very stable cooling and heating process (Figure S23). The PCMs sheets had high cycle performance because the main parameters (ΔH_m, ΔH_s and melting temperature values were listed on Figure S23) remained almost unchanged after 40 cycles.

2.3.2. Comparation with the important indicators in the literature

We made a comparison for the preparation method, melting enthalpy, *etc.* reported in the literature elsewhere to highlight the advantages of both PCM preparation method and enhanced phase transition performance (Table 2, Fig. 3g and Fig. 3h). Conventionally, PEG-based PCMs are usually fabricated by solvent casting, chemical cross-linking, and porous materials encapsulation. Notably, one of the typical advantages of the current study is the green and convenient preparation process. Moreover, as shown in Fig. 3g-h, both the enthalpies and the enthalpy efficiency are with the highest level as the reported in some recent works. All the above results support that the materials reported in current work have significant advantages in both preparation pathways and melting enthalpies. Notably, compared with the leakage poof PCM obtained by traditional chemical methods, this work will not involve the use of organic solvents. Moreover, biomass cyclodextrin is used, which improves the sustainability of the PCMs to a certain extent.

2.4. Heat response and process ability

Fig. 4a is the thermal response images of samples PPEG1-150, PPEG1.5–150, PPEG6-150, PPEG6-250 and PPEG6-350 on the hot plate at 85 °C. The specific temperature *vs.* time curves are shown in Fig. 4b and Fig. 4c. As it can be seen in Fig. 4b, PPEG1-150 presents two

Table 1
Some PCMs parameters.

Samples	Melting Enthalpy (J g^{-1})		Real enthalpy efficiency (EEr, %)	Extent of supercooling (°C)	Melting point (T_{peak}, °C)	Crystallinity (%)	Leakage
	Measured ΔH_m	Calculated ΔH_m					
PEG 1 k	166.4	–	–	8.7	38.5	84.7	Yes
PEG 1.5 k	167.4	–	–	5.7	49.5	85.2	Yes
PEG 6 k	176.2	–	–	22.5	58.5	89.7	Yes
PPEG6-30	116.1	95.5	130.7	7.4	66.3	79.5	No
PPEG6-60	123.7	110.6	122.1	7.9	61.2	79.6	No
PPEG6-90	126.8	121.0	114.6	9.5	62.4	78.3	No
PPEG6-120	127.8	128.5	108.4	8.9	62.2	76.7	No
PPEG6-150	133.9	134.2	108.2	9.2	61.8	78.7	No
PPEG6-200	140.1	141.2	106.7	11.1	63.9	80.2	No
PPEG6-250	151.2	146.2	110.5	9.9	64.7	85.1	No
PPEG6-300	158.7	150.0	112.4	9.7	61.0	88.2	No
PPEG6-350	162.2	152.9	112.1	9.1	63.1	90.8	No
PPEG1.5–150	133.4	128.4	107.8	−13.6	46.5, 54.0	78.4	No
PPEG1-150	129.8	129.0	104.9	−7.7	34.5, 56.8	76.2	No

Note: the extent of supercooling and crystallinity were both calculated according to the second heating and second cooling in DSC results. $\Delta H_{m,calcd.} = \omega_{PEG}\Delta H_{m,\ PEG} + \omega_{PLR}\Delta H_{m,\ PLR}$, where ω_{PEG} is the weight percentage of PEG, $\Delta H_{m,\ PEG}$ is the enthalpy of PEG, ω_{PLR} is the weight percentage of PLR, and $\Delta H_{m,\ PLR}$ is the enthalpy of PLR, with value of 71.3 J g^{-1}. [22].

Table 2
Methods and properties comparation about PEG or PEO based PCMs.

Composition	Methods	Solvents	Δ Hm (J g^{-1})	Enthalpy efficiency (%)	Reference
PEG/Halloysite nanotube	Melt-extrusion	–	96.80–115.90	>95.16	[28]
PEO/CNC	Solution mixing	H_2O	66.00–93.00	–	[29]
PEG/cellulose acetate/TDI	Electrospinning + crosslinking	Toluene, Acetone and N, N-dimethylacetamide	36.72–86.03	–	[30]
PEG/ PVA/Graphene aerogel	Sol-gel/hydrothermal reaction	H_2O	119.60–145.80	–	[31]
PEG/β-CD/MDI	Crosslinking copolymers	N, N-dimethylformamide	90.34–111.60	69.02–88.01	[32]
PEG/IPDI/f-PDAPs	Crosslinking	Methyl ethyl ketone	71.10–72.20	–	[33]
PEG/Xylitol/4, 4′-diphenylmethane diisocyanate	Crosslinking copolymers	–	68.40–80.46	–	[34]
Halloysite nanotubes/PEG/HDIB	Crosslinking copolymers	N, N-dimethylformamide	83.80–123.70	76.60–82.90	[35]
Graphene oxide/PEG/ HDIB	Crosslinking copolymers	N, N-dimethylformamide	71.70–78.00	52.47–57.32	[36]
PEG/IPDI/phloroglucinol	Crosslinking (PU)	Methyl ethyl ketone	117.10–146.60	–	[37]
PEG/glucose/4, 4′-diphenylmethane diisocyanate	Crosslinking (PU)	N, N-dimethylformamide	108.70–131.90	–	[19]
PEG/4, 4′-diphenylmethane diisocyanate /castor oil	Crosslinking (PU)	–	76.63–117.70	57.05–71.67	[38]
PEG/Ethylene gthylene	Hydrogel	H_2O	~100.00–150.00	–	[39]
PEG/CNT@Cr-MIL-101-NH_2	Physical blending and impregnating	Ethanol	83.10–124.90	–	[40]
PU/CNT (PEG + HDI for PCM)	Solution assisted infiltration	N, N-dimethylformamide	119.38–132.02	–	[41]
PEG + HDI + PNF	Linear PU	N-methyl-2-pyrrolidone	145.00–150.63	83.33–88.34	[42]
PEG + TDI + Melamine	Crosslinking	N, N-dimethylformamide	78.20–118.70	–	[43]
PEO/α-CD	Host-guest recognition	H_2O	57.11–104.29	92.79–99.87	[22]
PEO/α-CD/PEG	Blending	H_2O	116.10–162.20	(104.90–130.70)/ (133.90–395.30)	This work

Note: Cellulose nano crystal = CNC; Toluene diisocyanate = TDI; Polyvinyl alcohol = PVA; 4,4′-diphenylmethane diisocyanate = MDI; Hexamethylene Diisocyanate Biuret = HDIB; Phosphorylated polyvinyl alcohol = PPVA; f-PDAPs [32] = furan-modified polydopamine particles; Isophorone diisocyanate = IPDI; Carbon nanotube = CNT and PNF is phosphorene nanoflakes.

phase transition platforms of A1 (<40 °C) and A2 (<60 °C). In the curve of PPEG1.5–150, the B1 and B2 platforms are quite close. For sample PPEG6-150, the material maintains a relatively stable temperature for a long time from ~ 60 °C. The temperature rise of the PPEG6-150 sample is faster than that of the other two samples in the first 20 s because there is no phase transition for sample PPEG6-150 at the beginning. As soon as the plateau region passes, the sample continues to rise to the equilibrium temperature. Due to the delay of phase transition for a long time, the time to reach the equilibrium temperature for sample PPEG6-150 will lag behind the other two samples. Fig. 4c shows the temperature increasing curve of PPEG6-150, PPEG6-250 and PPEG6-350. In the initial stage, the heating rate is almost the same. The time for the three samples to enter the platform is quite similar. It can be further found that the phase change period increased with the increasing of PEG6k contents. This is because the higher latent heat, the longer the thermal control time under the condition of equal size, same heat source and similar thermal conductivity (the thermal conductivity of sample PPEG1-150, PPEG6-150 and PPEG6-250 are 0.31 ± 0.02 W/(m • K), 0.30 ± 0.05 W/(m • K) and 0.33 ± 0.03 W/(m • K), respectively). Specifically, there is a good linear relationship between the phase transition period (s) and the enthalpy (Fig. 4d), as described by the following equation (6):

$$\text{Phase change period} = 1.86\Delta H_m - 208.70, R^2 = 0.999 \quad (6)$$

where, phase change period is the time in the heating curves of PCM from beginning to the ending of phase change (Fig. 4c), and ΔH_m is the enthalpy of the PCM obtained by DSC test.

In addition, we found that the samples have thermoplastic properties. PPEG1-150 was selected as a typical representative to show the processing possibility and convenience of phase change materials. As shown in Fig. 4e-h, the sample is injectable, knittable, pelletizable and re-moldable. That is to say we can easily make filaments or pellets, which provides a convenient possibility for PCM to realize 3D printing.

Fig. 4i shows the elastic modulus G' and viscous modulus G" *vs.* strain of PPEG1-150, PPEG1.5–150 and PPEG6-150 at 80 °C. As seen in Fig. 4i, all the three samples show linear viscoelastic behavior at strain from 0.05 ~ 4 % under a frequency of 10 rad s^{-1} at 80 °C. Fig. 4j demonstrates the rheological data (G′ and G′′ *vs.* frequency) of the three PCMs with different PEG molecular weights at 80 °C. We found that both G′ and G′′ were independent upon the frequencies, and G′ was higher than G“ at all presented frequencies for all the three samples. This result confirms that these samples can be considered as gels [31]. The gel formation could be the result of the formation of PEO entanglement and α-CD crystal units. As seen in Fig. 4 j, G′ increased as the PEG molecule weight increased, indicating the stiffness of the samples increased when the PEG molecule weight increased. In addition, the crossover of G′ and G′′ were observed for all the three PCMs in the specific frequency region. Before the crossover, the PCM behaviors as viscous fluid. After the crossover, namelyω > 0.1 rad s^{-1} for PPEG6-150, ω>0.5 rad s^{-1} for PPEG1.5–150 andω > 10 rad s^{-1} for PPEG1-150 (point A, B and C in Fig. 4j), all the three PCMs behavior as elastic solid. Fig. 4k shows the rheological data of PPEG6-150, PPEG1.5–150 and PPEG1-150 samples (2 °C min^{-1}). The samples started to be soft after T_f, resulting in the jumping rheological data. The viscous flow temperature (T_f) was defined as the onset temperature at which G′ changed greatly during heating accordingly. The samples exhibited liquid states after T_f. As seen, the T_f values ranged from 95.4 to 124.1 °C, which are much higher than the melting temperature of PEG. Furthermore, it was found that the T_f value obviously increased with increasing the PEG molecular weight. We can assign that T_f is the minimum temperature for easy processing of materials. Because T_f (PPEG1-150) is 95.4 °C, this is the direct basis for us to select 100° C as the processing temperature of melt micro mixing extrusion of PPEG1-150 sample.

2.5. Application of the PCM

A typical application of phase change materials is the thermal management of electronic devices. As shown in Fig. 5a, phase change materials usually work with metal heatsink to regulate the temperature of solid state disk (SSD). In order to meet the needs of convenient laboratory testing, we designed a schematic structure (semi-SSD based device, Fig. 5b). As shown in Fig. 5b, the metal sheets (Copper sheet, 1

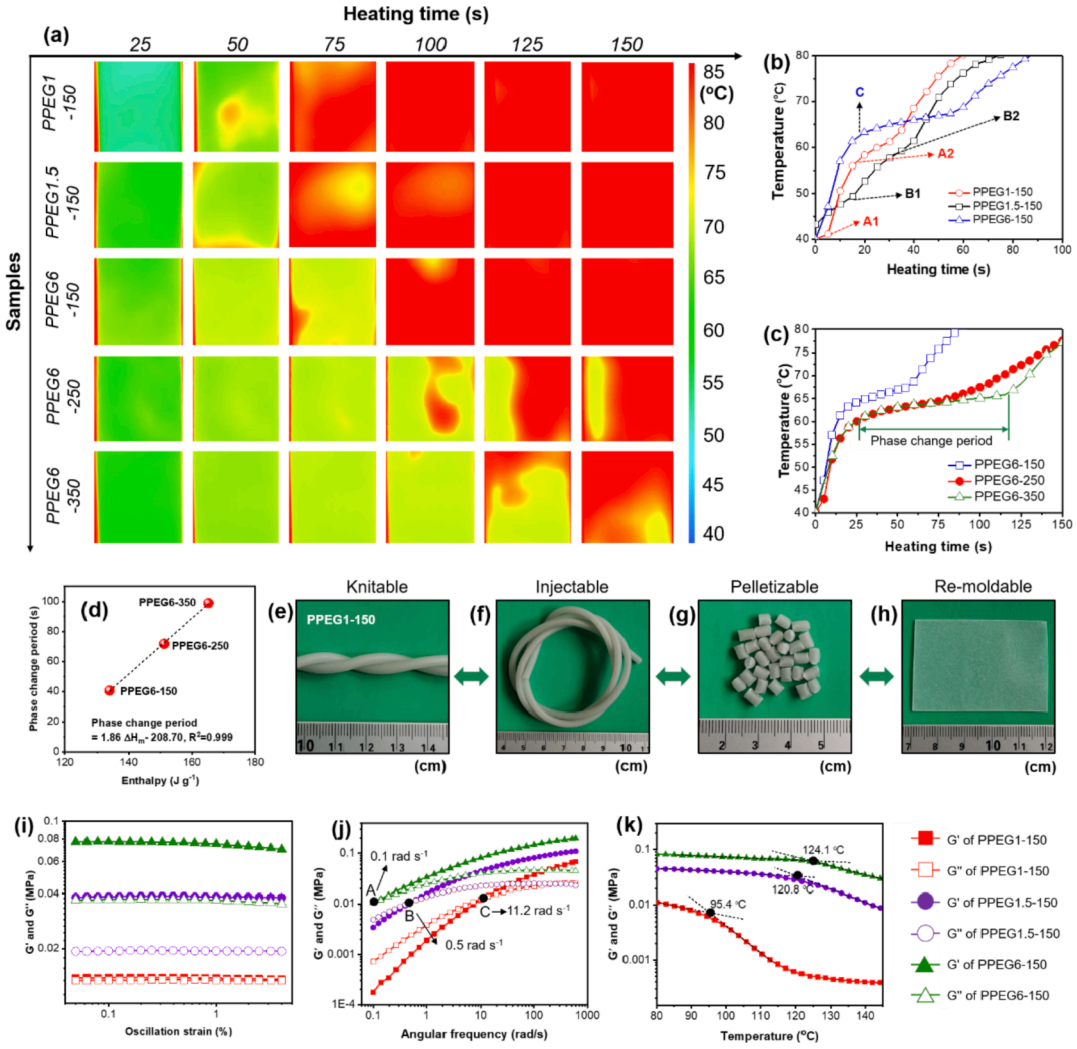

Fig. 4. (a) Thermal images of PPEG1-150, PPEG1.5–150, PPEG6-150, PPEG6-250 and PPEG6-350 during heating (all the samples have the same size of 20 mm × 20 mm × 1 mm), (b) the heating curves of samples PPEG1-150, PPEG1.5–150 and PPEG6-150, (c) the heating curves of sample PPEG6-150, PPEG6-250 and PPEG6-350, (d) phase change period *vs.* melting enthalpy plot, images for showing that the PCMs (taking sample PPEG1-150 as a typical example) are (e) Knitable, (f) Injectable or extrudable (at 100 °C), (g) Palletizable and (h) Re-moldable (at 100 °C), (i) the elastic modulus G′ and viscous modulus G″ *vs.* strain (%) of PPEG1-150, PPEG1.5–150 and PPEG6-150 at 80 °C, (j) G′ and G″ *vs.* frequency of PPEG1-150, PPEG1.5–150 and PPEG6-150 at 80 °C, and (k) G′ and G″ *vs.* temperature curves of PPEG1-150, PPEG1.5–150 and PPEG6-150 at a heating rate of 2 °C min^{-1} from 80 °C to 145 °C.

mm in thickness), protecting sheet (Polypropylene (PP) with 2 mm in thickness), PCM (70 mm × 22 mm × 1 mm in thickness, which is the same as the size of commercial product) and the top metal heatsink stacked together from the bottom to the top. Fig. 5c shows the schematic diagram of the whole material test system. Fig. 5d is a top view photograph of two schematic devices with PCM (following the stacking structure shown in Fig. 5b). The specific images of PCM samples (both commercial one and sample PPEG6-350) with the calculated thermal absorption capacities is shown in Figure S24. Fig. 5e shows the IR images of different samples at different heating time. We can further obtain the measured temperature change heating curves, as shown in Fig. 5f.

As shown in Fig. 5f and Fig. 5g, the endothermic and exothermic state of the analog device can form a relatively stable equilibrium state at last. During the whole heating cycle, sample PPEG6-350 in this study showed significantly better temperature control state than both the blank samples and commodities. Specifically, the temperature of the protecting part with PCM was significantly lower than that of blank sample and commercial PCM. Furthermore, there was no significant difference in the initial stage (I, linear heating stage, Fig. 5g). When entering the phase transition region (region II), the temperature difference gradually appears and maintain between 5 and 6 °C for ~ 30 min. The difference is due to the high enthalpy effect of PPEG6-350 phase transition, which plays a role in temperature regulation for a long time. When the phase transformation reaches the capacity, that is, PCM melts totally, the heat absorption of the material will be absorbed in the form of sensible heat, which will increase the temperature and approach the equilibrium temperature finally. This is also the reason why in Fig. 5f and 5 g, the temperature of the third stage (III) is close to the commodity or blank sample. The DSC curve of the commercial PCM is given in Figure S25. It can be found that the latent heat of PCM is very small. Therefore, the thermal control mainly depends on its heat conduction to the soaking plate to achieve heat dissipation. In this study, the significant existence of temperature difference for a long time fully proves the significant utility of PCM. At the same time, it also shows the practical significance of PCM in the field of thermal control of electronic devices. We expect that under the premise of maintaining high latent heat, and then further improve the thermal conductivity of the material, it is expected that more significant heat management effect will be achieved. The corresponding work will continue to be reported in the near future.

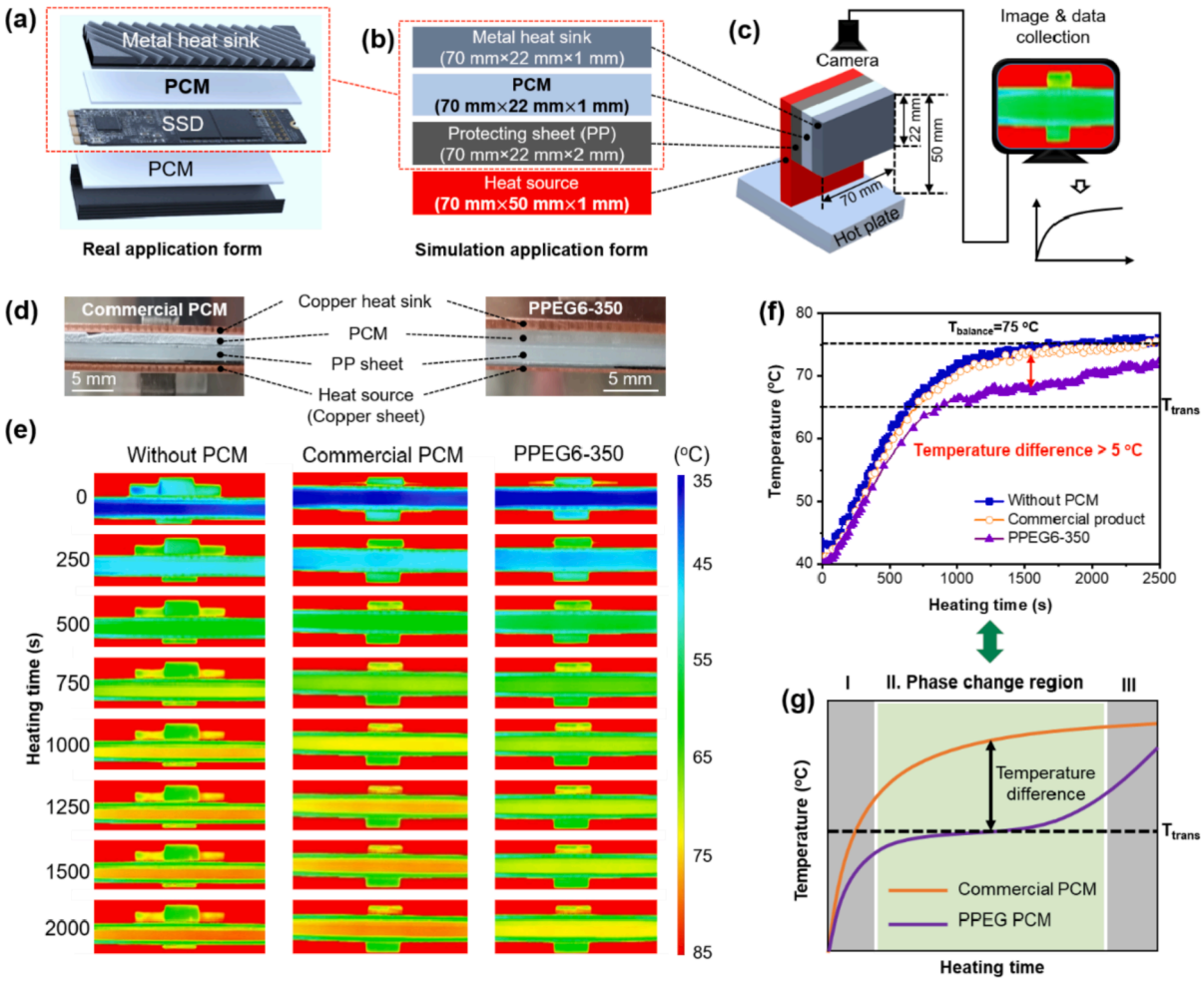

Fig. 5. (a) Real application form of the PCM for SSD thermal management, (b) illustration of the experimental stack structure of the device, (c) test process and sample test diagram: including sample heating, signal acquisition and data storage, (d) the structure diagram of the designed device, (e) IR images of the devices during heating at 85 °C, (f) the heating curves of the devices that without PCM, with commercial PCM sample, and with PPEG6-350, and (g) the general heating curves illustration of the devices that with commercial sample, and PCM with high enthalpy.

3. Conclusion

In this work, we realized supramolecular PLR as the support material to encapsulate different molecular weight and different content of PEG to prepare high performance phase change materials. The α-CD crystal units can keep the shape during melting of PEG and act as the physical crosslinking point. The structural similarity between PLR and PEG ensures the compatibility between PLR and PEG, so there is no leakage of PEG (Mn > 1304 g mol^{-1}) during the phase transition. PLR/PEG PCMs can ensure the shape stability within PEG contents of 30 wt% – 350 wt %. In addition, by introducing PEG with different molecular weight, the phase transition temperature can be adjustable from 30 °C to 60 °C. The enthalpy of phase transition can be adjustable from 116.1 to 162.2 J g^{-1}. Because the molecular chains promote each other and the support material itself is also a phase change material, the enthalpy efficiency is significantly higher than 100%. For sample PPEG1-150 and PPEG1.5–150, the supercooling was calculated as −13.62 °C and −7.66 °C, respectively. These materials can be used as thermal control sheets for electronic devices such as SSD. Compared with commercial PCM, the PPEG6-350 has better temperature control effect (There is usually a temperature difference of>5 °C) on the heating device in a certain time range. This work provides a basis for the development of simple, efficient, green and high-performance PEG based phase change materials. Moreover, the excellent process ability has laid a solid foundation for its industrial application.

CRediT authorship contribution statement

Guang-Zhong Yin: Conceptualization, Methodology, Data curation, Writing – original draft, Writing – review & editing. **Alba Marta López:** Data curation, Methodology, Writing – review & editing. **Xiao-Mei Yang:** Data curation, Writing – review & editing. **Xiang Ao:** Data curation, Writing – review & editing. **Jose Hobson:** Data curation, Writing – review & editing. **De-Yi Wang:** Methodology, Writing – review & editing, Supervision, Funding acquisition.

Declaration of Competing Interest

The authors declare that they have no known competing financial interests or personal relationships that could have appeared to influence the work reported in this paper.

Acknowledgment

This work was supported by BIOFIRESAFE Project funded by Ministerio De Ciencia E Innovación (MINECO), Spain with Project number: PID2020-117274RB-I00BIOFIRESAFE.

Appendix A. Supplementary data

Supplementary data to this article can be found online at https://doi.

org/10.1016/j.cej.2022.136421.

References

[1] Y. Luo, Y. Xie, H. Jiang, Y. Chen, L. Zhang, X. Sheng, D. Xie, H. Wu, Y. Mei, Flame-retardant and form-stable phase change composites based on MXene with high thermostability and thermal conductivity for thermal energy storage, Chem. Eng. J. 420 (2021), 130466.

[2] P. Min, J. Liu, X. Li, F. An, P. Liu, Y. Shen, N. Koratkar, Z.-Z. Yu, Thermally Conductive Phase Change Composites Featuring Anisotropic Graphene Aerogels for Real-Time and Fast-Charging Solar-Thermal Energy Conversion, Adv. Funct. Mater. 28 (51) (2018) 1805365.

[3] L. Li, C. Xu, R. Chang, C. Yang, C. Jia, L. Wang, J. Song, Z. Li, F. Zhang, B. Fang, X. Wei, H. Wang, Q. Wu, Z. Chen, X. He, X. Feng, H. Wu, M. Ouyang, Thermal-responsive, super-strong, ultrathin firewalls for quenching thermal runaway in high-energy battery modules, Energy Storage Mater. 40 (2021) 329–336.

[4] M. Mehrali, J.E. ten Elshof, M. Shahi, A. Mahmoudi, Simultaneous solar-thermal energy harvesting and storage via shape stabilized salt hydrate phase change material, Chem. Eng. J. 405 (2021), 126624.

[5] W. Aftab, X. Huang, W. Wu, Z. Liang, A. Mahmood, R. Zou, Nanoconfined phase change materials for thermal energy applications, Energy Environ. Sci. 11 (6) (2018) 1392–1424.

[6] D.G. Atinafu, S.J. Chang, K.-H. Kim, W. Dong, S. Kim, A novel enhancement of shape/thermal stability and energy-storage capacity of phase change materials through the formation of composites with 3D porous (3,6)-connected metal–organic framework, Chem. Eng. J. 389 (2020), 124430.

[7] Z. Sun, Z. Han, H. Liu, D. Wu, X. Wang, Nanoflaky nickel-hydroxide-decorated phase-change microcapsules as smart electrode materials with thermal self-regulation function for supercapacitor application, Renewable Energy 174 (2021) 557–572.

[8] A. Bashiri Rezaie, M. Montazer, Shape-stable thermo-responsive nano Fe3O4/fatty acids/PET composite phase-change material for thermal energy management and saving applications, Appl. Energy 262 (2020), 114501.

[9] L. Cheng, L. Kong, X. Zhang, X. Kong, Form-stable phase change nanocapsules with photo and electric dual responses for multipurpose applications in energy storage and conversion, Sol. Energy Mater. Sol. Cells 235 (2022), 111461.

[10] L. Feng, S. Dong, H. Zhou, L. Yang, F. Yuan, Y. Yang, J. Lei, L. Bao, L. Bian, J. Wang, n-Dodecanol nanocapsules with supramolecular lock shell layer for thermal energy storage, Chem. Eng. J. 389 (2020), 124483.

[11] X. Huang, J. Guo, Y. Gong, S. Li, S. Mu, S. Zhang, In-situ preparation of a shape stable phase change material, Renewable Energy 108 (2017) 244–249.

[12] L. Kong, X. Kong, Z. Ji, X. Wang, X. Zhang, Large-Scale Fabrication of a Robust Superhydrophobic Thermal Energy Storage Sprayable Coating Based on Polymer Nanotubes, ACS Appl. Mater. Interfaces 12 (44) (2020) 49694–49704.

[13] F. Xue, Y. Lu, X.-D. Qi, J.-H. Yang, Y. Wang, Melamine foam-templated graphene nanoplatelet framework toward phase change materials with multiple energy conversion abilities, Chem. Eng. J. 365 (2019) 20–29.

[14] X. Zhang, N. Li, Z. Hu, J. Yu, Y. Wang, J. Zhu, Direct fabrication of poly(p-phenylene terephthalamide) aerogel and its composites with great thermal insulation and infrared stealth, Chem. Eng. J. 388 (2020), 124310.

[15] L. Zhou, L.-S. Tang, X.-F. Tao, J. Yang, M.-B. Yang, W. Yang, Facile fabrication of shape-stabilized polyethylene glycol/cellulose nanocrystal phase change materials based on thiol-ene click chemistry and solvent exchange, Chem. Eng. J. 396 (2020), 125206.

[16] G.-Z. Yin, X.-M. Yang, Biodegradable polymers: a cure for the planet, but a long way to go, J. Polym. Res. 27 (2) (2020) 38.

[17] D.G. Atinafu, S. Jin Chang, K.-H. Kim, S. Kim, Tuning surface functionality of standard biochars and the resulting uplift capacity of loading/energy storage for organic phase change materials, Chem. Eng. J. 394 (2020), 125049.

[18] P. Yuan, P. Zhang, T. Liang, S. Zhai, Effects of surface functionalization on thermal and mechanical properties of graphene/polyethylene glycol composite phase change materials, Appl. Surf. Sci. 485 (2019) 402–412.

[19] C. Chen, W. Liu, Z. Wang, K. Peng, W. Pan, Q. Xie, Novel form stable phase change materials based on the composites of polyethylene glycol/polymeric solid-solid phase change material, Sol. Energy Mater. Sol. Cells 134 (2015) 80–88.

[20] Y. Zhang, L. Wang, B. Tang, R. Lu, S. Zhang, Form-stable phase change materials with high phase change enthalpy from the composite of paraffin and cross-linking phase change structure, Appl. Energy 184 (2016) 241–246.

[21] C. Chen, J. Chen, Y. Jia, P.D. Topham, L. Wang, Binary shape-stabilized phase change materials based on poly(ethylene glycol)/polyurethane composite with dual-phase transition, J. Mater. Sci. 53 (24) (2018) 16539–16556.

[22] G.-Z. Yin, J. Hobson, Y. Duan, D.-Y. Wang, Polyrotaxane: New generation of sustainable, ultra-flexible, form-stable and smart phase change materials, Energy Storage Mater. 40 (2021) 347–357.

[23] Y. Xia, H. Zhang, P. Huang, C. Huang, F. Xu, Y. Zou, H. Chu, E. Yan, L. Sun, Graphene-oxide-induced lamellar structures used to fabricate novel composite solid-solid phase change materials for thermal energy storage, Chem. Eng. J. 362 (2019) 909–920.

[24] S. Uenuma, R. Maeda, H. Yokoyama, K. Ito, Formation of Isolated Pseudo-Polyrotaxane Nanosheet Consisting of α-Cyclodextrin and Poly(ethylene glycol), Macromolecules 52 (10) (2019) 3881–3887.

[25] C.L. Jackson, G.B. McKenna, The melting behavior of organic materials confined in porous solids, J. Chem. Phys. 93 (12) (1990) 9002–9011.

[26] X. Zhang, H. Liu, Z. Huang, Z. Yin, R. Wen, X. Min, Y. Huang, Y. Liu, M. Fang, X. Wu, Preparation and characterization of the properties of polyethylene glycol @ Si3N4 nanowires as phase-change materials, Chem. Eng. J. 301 (2016) 229–237.

[27] P. Cheng, H. Gao, X. Chen, Y. Chen, M. Han, L. Xing, P. Liu, G. Wang, Flexible monolithic phase change material based on carbon nanotubes/chitosan/poly(vinyl alcohol), Chem. Eng. J. 397 (2020), 125330.

[28] S. Thanakkasaranee, J. Seo, Effect of halloysite nanotubes on shape stabilities of polyethylene glycol-based composite phase change materials, Int. J. Heat Mass Transf. 132 (2019) 154–161.

[29] Z. Shi, H. Xu, Q. Yang, C. Xiong, M. Zhao, K. Kobayashi, T. Saito, A. Isogai, Carboxylated nanocellulose/poly(ethylene oxide) composite films as solid–solid phase-change materials for thermal energy storage, Carbohydr. Polym. 225 (2019), 115215.

[30] C. Chen, L. Wang, Y. Huang, Crosslinking of the electrospun polyethylene glycol/cellulose acetate composite fibers as shape-stabilized phase change materials, Mater. Lett. 63 (5) (2009) 569–571.

[31] J. Shen, P. Zhang, L. Song, J. Li, B. Ji, J. Li, L. Chen, Polyethylene glycol supported by phosphorylated polyvinyl alcohol/graphene aerogel as a high thermal stability phase change material, Compos. B Eng. 179 (2019), 107545.

[32] K. Peng, C. Chen, W. Pan, W. Liu, Z. Wang, L. Zhu, Preparation and properties of β-cyclodextrin/4,4′-diphenylmethane diisocyanate/polyethylene glycol (β-CD/MDI/PEG) crosslinking copolymers as polymeric solid–solid phase change materials, Sol. Energy Mater. Sol. Cells 145 (2016) 238–247.

[33] S. Yang, X. Du, S. Deng, J. Qiu, Z. Du, X. Cheng, H. Wang, Recyclable and self-healing polyurethane composites based on Diels-Alder reaction for efficient solar-to-thermal energy storage, Chem. Eng. J. 398 (2020), 125654.

[34] Y. Yang, W. Kong, X. Cai, Solvent-free preparation and performance of novel xylitol based solid-solid phase change materials for thermal energy storage, Energy Build. 158 (2018) 37–42.

[35] Y. Zhou, D. Sheng, X. Liu, C. Lin, F. Ji, L. Dong, S. Xu, Y. Yang, Synthesis and properties of crosslinking halloysite nanotubes/polyurethane-based solid-solid phase change materials, Sol. Energy Mater. Sol. Cells 174 (2018) 84–93.

[36] Y. Zhou, X. Liu, D. Sheng, C. Lin, F. Ji, L. Dong, S. Xu, H. Wu, Y. Yang, Graphene oxide/polyurethane-based solid–solid phase change materials with enhanced mechanical properties, Thermochim Acta 658 (2017) 38–46.

[37] S. Sundararajan, A.B. Samui, P.S. Kulkarni, Thermal Energy Storage Using Poly (ethylene glycol) Incorporated Hyperbranched Polyurethane as Solid-Solid Phase Change Material, Ind. Eng. Chem. Res. 56 (49) (2017) 14401–14409.

[38] Z. Liu, X. Fu, L. Jiang, B. Wu, J. Wang, J. Lei, Solvent-free synthesis and properties of novel solid–solid phase change materials with biodegradable castor oil for thermal energy storage, Sol. Energy Mater. Sol. Cells 147 (2016) 177–184.

[39] Q. Sun, H. Zhang, J. Xue, X. Yu, Y. Yuan, X. Cao, Flexible phase change materials for thermal storage and temperature control, Chem. Eng. J. 353 (2018) 920–929.

[40] J. Wang, X. Huang, H. Gao, A. Li, C. Wang, Construction of CNT@Cr-MIL-101-NH2 hybrid composite for shape-stabilized phase change materials with enhanced thermal conductivity, Chem. Eng. J. 350 (2018) 164–172.

[41] W. Aftab, A. Mahmood, W. Guo, M. Yousaf, H. Tabassum, X. Huang, Z. Liang, A. Cao, R. Zou, Polyurethane-based flexible and conductive phase change composites for energy conversion and storage, Energy Storage Mater. 20 (2019) 401–409.

[42] W. Aftab, M. Khurram, S. Jinming, H. Tabassum, Z. Liang, A. Usman, W. Guo, X. Huang, W. Wu, R. Yao, Q. Yan, R. Zou, Highly efficient solar-thermal storage coating based on phosphorene encapsulated phase change materials, Energy Storage Mater. 32 (2020) 199–207.

[43] Y. Kou, K. Sun, J. Luo, F. Zhou, H. Huang, Z.-S. Wu, Q. Shi, An intrinsically flexible phase change film for wearable thermal managements, Energy Storage Mater. 34 (2021) 508–514.